

THE SAHARAN AIR LAYER AND THE FATE OF AFRICAN EASTERLY WAVES

NASA's AMMA Field Study of Tropical Cyclogenesis

BY EDWARD J. ZIPSER, CYNTHIA H. TWOHY, SI-CHEE TSAY, K. LEE THORNHILL, SIMONE TANELLI, ROBERT ROSS, T. N. KRISHNAMURTI, Q. JI, GREGORY JENKINS, SYED ISMAIL, N. CHRISTINA HSU, ROBBIE HOOD, GERALD M. HEYMSFIELD, ANDREW HEYMSFIELD, JEFFREY HALVERSON, H. MICHAEL GOODMAN, RICHARD FERRARE, JASON P. DUNION, MICHAEL DOUGLAS, ROBERT CIFELLI, GAO CHEN, EDWARD V. BROWELL, AND BRUCE ANDERSON

The objectives of an extensive field campaign based from the Cape Verde islands, Africa and Barbados during August–September 2006 included distinguishing disturbances that become tropical cyclones from those that do not.

The major hurricanes that affect the United States often can be traced back to weak disturbances moving westward across the tropical Atlantic Ocean. These are wavelike disturbances in the low-level tropical easterlies, with a horizontal scale of a few thousand kilometers and a period of 4–5 days, giving rise to the terminology “easterly wave” as described, for example, by Riehl (1954), mostly based upon observations in the Caribbean region. In recent years it

has become clear that the structure of the waves over and near Africa often differs from that in the western Atlantic, so they are usually called African easterly waves (AEWs). They are known to originate over the African continent, with their initial growth fueled by the temperature contrast between the hot air over the Sahara desert and the relatively cooler, humid air to its south. This temperature gradient is persistent, so it is logical that these AEWs emerge out of Africa

AFFILIATIONS: ZIPSER—University of Utah, Salt Lake City, Utah; TWOHY—Oregon State University, Corvallis, Oregon; TSAY, HSU, AND G. HEYMSFIELD—NASA Goddard Space Flight Center, Greenbelt, Maryland; THORNHILL—Science Systems and Applications, Inc., Lanham, Maryland; TANELLI—Jet Propulsion Laboratory, California Institute of Technology, Pasadena, California; ROSS AND KRISHNAMURTI—The Florida State University, Tallahassee, Florida; JI—Earth System Science Interdisciplinary Center, University of Maryland, College Park, College Park, Maryland; JENKINS—Howard University, Washington, D.C.; ISMAIL, FERRARE, CHEN, BROWELL, AND ANDERSON—NASA Langley Research Center, Hampton, Virginia; HOOD AND GOODMAN—NASA Marshall Space Flight Center, Huntsville, Alabama; A. HEYMSFIELD—National Center for Atmospheric Research, Boulder, Colorado; HALVERSON—University of

Maryland, Baltimore County, Baltimore, Maryland; DUNION—NOAA/AOML/Hurricane Research Division, Miami, Florida; DOUGLAS—NOAA/National Severe Storms Laboratory, Norman, Oklahoma; CIFELLI—Colorado State University, Fort Collins, Colorado

CORRESPONDING AUTHOR: Edward J. Zipser, Department of Meteorology, University of Utah, Salt Lake City, UT 84112-0110
E-mail: ed.zipser@utah.edu

The abstract for this article can be found in this issue, following the table of contents.

DOI:10.1175/2009BAMS2728.1

In final form 4 February 2009
©2009 American Meteorological Society

with great regularity throughout the summer and early fall; however, only a small fraction strengthen into tropical storms or hurricanes, and distinguishing those special few from all of the harmless AEWs is of great practical importance and has been a long-standing scientific mystery.

The fate of AEWs is a component of a more general puzzle, that is, why do some tropical disturbances intensify into hurricanes, whereas most do not? One might suppose that the most obvious region to study to seek a solution would be the east-central Atlantic, precisely because of the regular progression of AEWs through a limited domain. The isolation of this region places it out of range of research aircraft based in the western Atlantic. One must go back in time to 1974, when a massive field program to study tropical convection and rainfall covered this region with ships and aircraft [the Global Atmospheric Research Program (GARP) Atlantic Tropical Experiment (GATE); see Kuettner and Parker 1976; Houze and Betts 1981]. Indeed, some of the most valuable research on AEWs uses data from this program (e.g., Reed et al. 1977), but with little or no attention focused on the question of which AEWs might evolve into tropical cyclones (TCs). It would be 32 yr before a field program returned to the east Atlantic to seek an answer.

BACKGROUND AND MOTIVATION. The African Monsoon Multidisciplinary Analysis (AMMA), a large international project to improve the understanding of the West African monsoon (Redelsperger et al. 2006), created the opportunity for a field program in the east Atlantic in 2006. With AMMA providing data over a vast area of West Africa, National Aeronautics and Space Administration (NASA) was able to extend that database westward over the Atlantic with their field program [NASA-AMMA (NAMMA)] based mainly on Cape Verde's islands during August and September, whereas the National Oceanic and Atmospheric Administration (NOAA) further extended that east-west coverage with research aircraft operating out of Barbados. Although the surface-based radiosonde network over the Atlantic did not rival that in GATE, three decades of progress in remote sensing from satellites and aircraft, and in multiscale numerical simulation, led to a different but effective comprehensive analysis. At the same time, these improvements have led to significant new knowledge that has updated and refocused the scientific questions.

In recent years, the availability of multidecadal reanalyses using both National Centers for Environmental Prediction (NCEP) and European Centre

for Medium-Range Weather Forecasts [ECMWF; 40-yr ECMWF Re-Analysis (ERA-40)] model data have been widely used to track and analyze tropical disturbances in general and AEWs in particular. Although early studies by Carlson (1969) and Burpee (1974) recognized that there were often two preferred tracks of AEWs emerging from Africa (north and south of 15°N), Thorncroft and Hodges (2001), Fink et al. (2004), and Chen (2006) used ERA-40 to demonstrate that the northern systems were typically at low levels and dry, whereas the southern systems typically were in the midtroposphere and rainy. If and how these two systems merge over the Atlantic is still questionable, and the central question of how to recognize AEWs that are more likely to evolve into TCs is still debatable.

There have been important recent advances in the capabilities of satellite remote sensing to detect and track the ubiquitous outbreaks of dust that emerge out of Africa. As early as Carlson and Prospero (1972), these massive dust outbreaks were tracked to the Caribbean, Florida, and beyond. However, their frequency and regularity has stimulated many to ask whether they have an influence on AEWs and tropical cyclogenesis. The dust outbreaks are usually associated with hot, dry air, dubbed the Saharan air layer (SAL). Karyampudi and Carlson (1988) concluded that the SAL is important, if not necessary, in the initial development of AEWs. Karyampudi and Pierce (2002) found that the SAL had a positive influence on the genesis of two Atlantic storms through the enhancement of baroclinic instability. Dunion and Velden (2004) proposed that the SAL can inhibit tropical TC intensity but is primarily due to the stabilizing effect of the warm, dry air and enhanced vertical wind shear. They suggested that any direct influence of the dust on TC development was not yet fully understood. Others have proposed that the dust may directly affect cloud microphysics by reducing precipitation efficiency (Rosenfeld et al. 2001) or by enhancing convective intensity (Khain et al. 2005; Jenkins et al. 2008), although it is not at all clear how such changes in microphysics would affect tropical cyclogenesis.

Other studies have suggested that African dust loading over the Atlantic might play an important role in the activity level of a hurricane season. Evan et al. (2006) conducted a 25-yr study that showed a strong relationship between interannual variations in North Atlantic TC activity and atmospheric dust cover over the main development region. This has become an active research area, for example, see Zhang et al. (2007), Evan et al. (2008), and Wong et al. (2008). Lau and Kim (2007a,b,c) indicated that

the excess of Saharan dust in the 2006 premonsoon season, as compared to 2005, was largely responsible for chilling the sea surface temperature in the North Atlantic, possibly contributing to the big decrease in TC activity from 2005 to 2006. Daily retrievals of aerosol properties over the NAMMA domain of interest are achieved by employing the Deep Blue algorithm (Hsu et al. 2004) using measurements from the Moderate Resolution Imaging Spectroradiometer (MODIS) onboard NASA's Earth Observing System (EOS) *Aqua* satellite. Figure 1 depicts the spatial distribution of Saharan dust loading (aerosol optical thickness τ at 0.55- μm wavelength) from source regions to downwind transport pathways during the NAMMA intensive observational period (e.g., 15 August–15 September 2006). Throughout the NAMMA field campaign, these retrievals were used as a tool to help study how the SAL affects the life cycle of an individual AEW, whether by dust effects, the hot dry air, enhanced vertical wind shear, or a combination of these factors. NAMMA used the islands of Sal and Praia near 23°W in the nation of Cape Verde as a base of operations to help fill the large data void over the east Atlantic during the summer of 2006.

SCIENTIFIC OBJECTIVES. To gain an improved understanding of the linkage between AEWs, the SAL, and tropical cyclogenesis, the NAMMA field campaign sought to address a number of key scientific questions posed by both NASA and NOAA investigators. Specifically,

- What is the essential difference between AEWs that develop into TCs and those that do not? To what extent is tropical cyclogenesis controlled by the structure and intensity of the large-scale wave versus the smaller-scale convective systems that erupt periodically within the wave and its constituent low-level vorticity centers?
- What is the specific role of the SAL in the fate of the AEWs and TCs? Does the African dust have a direct inhibiting effect on the attempt of the circulation to form and intensify? Are the most important influences of the SAL the ingestion of dry air into the wave and perhaps enhanced vertical

wind shear? Or does the dust play its role through influencing cloud microphysics, cloud condensation and ice nuclei, and liquid and ice particle size distributions in ways that mitigate or redistribute precipitation and latent heating in the storm?

- What is the characteristic vertical distribution, microphysical and optical properties, and composition of the African dust, and in what specific ways does the dust affect cloud microphysics and cloud dynamics?

STRATEGY IN THE FIELD. The NAMMA campaign was designed to be complementary with, and extend the downwind reach of, the international AMMA experimental network located across pan-equatorial Africa. It was also designed to fill a critical void in the in situ observation of AEWs located between mainland Africa and the eastward range limit of NOAA's research aircraft that were coordinating research missions from Barbados. These missions, conducted by the NOAA Hurricane Research Division (HRD), do not normally fly beyond the central Atlantic. Cape Verde's islands provided an ideal "perch" from which to base the NASA DC-8 within this data-sparse region. Cape Verde also provided an additional sampling location for radar observations of AEWs, establishing the westernmost end of a chain of Doppler radars extending from the interior of Africa [the Massachusetts Institute of Technology (MIT) radar located in Niamey, Niger] to the coastal

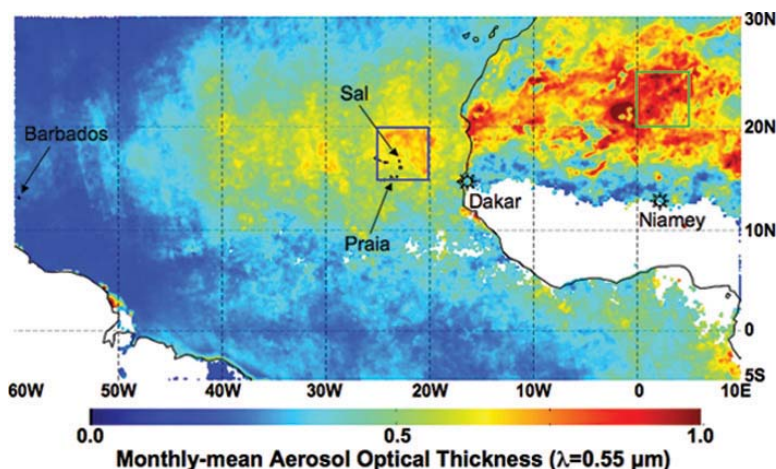


FIG. 1. Monthly-mean (15 Aug–15 Sep 2006) aerosol optical thickness retrieved by using the Deep Blue algorithm for EOS/*Aqua* MODIS measurements over the NAMMA research domain. The locations (Niamey, Dakar, Sal, Praia, and Barbados) are indicated. To exclude cloud contamination (white shading), at least 5 days of cloud-free data per 0.1° square is required for computing the monthly mean. As expected, the dust loading is lower over the ocean ($\tau = 0.647 \pm 0.057$, blue box) than over African source regions ($\tau = 0.832 \pm 0.116$, green box).

zone [the NASA polarimetric radar (NPOL), located at Kawsara near Dakar, Senegal] and to the open ocean [the NASA Tropical Ocean and Global Atmosphere (TOGA) radar located at Praia, Cape Verde]. One important goal of these radars was to sample the transition of AEWs and their embedded convection from a purely continental to a purely oceanic regime and to note any linkage between the intensity and distribution of convective versus stratiform rainfall and the process of (or the lack thereof) tropical cyclogenesis. Table 1 lists the instrumentation for NAMMA.

Mission strategies involving the DC-8 encompassed numerous objectives. First and foremost, the DC-8 was tasked to sample numerous AEWs as they emerged off of the African coast and moved over the eastern North Atlantic, following the wave on successive days, including both developing and nondeveloping systems. Dropwindsondes from the DC-8, high-frequency rawinsondes from Praia, and enhanced rawinsondes and pibals from West Africa were used to map the wind and thermodynamic structure of these AEWs. Additionally, the DC-8 intensively sampled the SAL, and, most importantly, the highly dynamic interface between the SAL and AEWs. During one mission, the DC-8 flew instrument intercomparison flight legs alongside the U.K. BAe-146 research aircraft, acquiring a detailed set of in situ observations of aerosol size distribution and vertical aerosol structure within the SAL. The U.K. group's 2006 program follows extensive results on direct sampling of Sahara dust reported previously from the Saharan Dust Experiment (SHADE), see for example, Haywood et al. (2003), Highwood et al. (2003), and Tanré et al. (2003). The intercomparisons during NAMMA allow for a way to unify the data from the two aircraft platforms and campaigns, which will enhance the science value of each of the two datasets and provide a broader science perspective of the Saharan dust layers. On several occasions, AEWs that had already formed into a TC, that were actively undergoing cyclogenesis, or that had intensity change were handed off further downstream from the NOAA research aircraft operating from Barbados to maintain the continuity of sampling across the Atlantic basin. A final mode of aircraft observations involved using the DC-8 for satellite calibration-validation. Several missions were timed such that the aircraft would underfly the NASA A-Train of remote sensors, during the ferry either to or from the scientific target of interest. The suite of instrument platforms on the DC-8—including humidity, aerosol, cloud particle and temperature profilers, and numerous in situ probes—provided targeted validation data for the satellite observations.

SUMMARY OF MAJOR ACCOMPLISHMENTS. The Atlantic hurricane season of 2006 was less active than the long-term mean, in sharp contrast to the record-shattering season of 2005. However, the AEWs developed and emerged

TABLE 1. NAMMA instrumentation.

Instrument	Principal investigators	Sensor type	Description of parameters measured and/or derived	Platform/location
NPOL	J. Gerlach/NASA, P. Kucera/NCAR	Dual-polarized S-band Doppler radar	Radar reflectivity, radial velocity, and rainfall estimates and rates	Near Dakar, Senegal
Radiosonde/tethersonde	E. Joseph/HU, G. Jenkins/HU, J. Fuentes/UVA	Balloon-borne sondes and tethersonde	Vertical temperature, wind, and humidity profiles	Near Dakar, Senegal
Optical theodolite	M. Douglas/NOAA	Pilot balloons	Winds aloft	West Africa
Radiosonde	F. Schmidlin/NASA	Balloon-borne sondes	Vertical temperature, wind, and humidity profiles	Praia, Cape Verde
SMART and COMMIT	Q. Ji/University of Maryland, S.-C. Tsay/NASA	Radiometer (solar, IR, microwave), spectrometer; lidar; meteorological surface probe, particle sizer, gas monitor, nephelometer, aethalometer	Atmospheric state (temperature, precipitation RH, wind, rain rate), particle size (1–15 μm), PM10 mass CO, CO ₂ , SO ₂ , NO _x , O ₃ , sky image, temperature and water vapor profile, aerosol scattering and absorption coefficient, extinction profile, and cloud and dust properties	Sal, Cape Verde
TOGA radar	J. Gerlach/NASA, R. Cifelli/University of North Dakota	C-band Doppler radar	Radar reflectivity, radial velocity, spectral width, and rainfall estimates and rates	Praia, Cape Verde

Sferics Timing and Ranging Network (STARNET) long-range lightning monitoring network	E. Williams/MIT, M. Anagnostou/University of Connecticut	Very long frequency sferics array	Identifies location and polarity of lightning	Africa
2D stereo (2D-S)	P. Lawson/SPEC, Inc.	Cloud particle sizing and imaging	Particle size distribution, concentration, ice water content, and particle shape	DC-8
Cloud aerosol precipitation spectrometer (CAPS)	A. Heymsfield/NCAR	Optical array imaging probe and scattering spectrometer	Particle size distribution, ice water content, extinction, radar reflectivity, and fall velocity	DC-8
Carbon Monoxide By Attenuation of Laser Transmission (COBALT)	J. Podolske/NASA	In situ laser absorption spectrometer	Carbon monoxide mixing ratio	DC-8
Cloud particle imager (CPI)	P. Lawson/SPEC, Inc.	Cloud particle sizing and imaging	Particle size distribution, ice water content, extinction, radar reflectivity, and fall velocity	DC-8
CVI	C. Twohy/Oregon State University	In situ droplet impactor	Cloud and total condensate water content, and nuclei composition	DC-8
Diode laser hygrometer (DLH)	G. Diskin/NASA	In situ laser absorption spectrometer	Water vapor mixing ratio, flux, partial pressure, and relative humidity	DC-8
Dual frequency airborne precipitation radiometer	E. Im, S. Durden, and S. Tanelli/Jet Propulsion Lab	13.4/35.6-GHz scanning, Doppler, polarimetric radar	3D volumes of radar backscatter, Doppler velocity, and linear depolarization ratio: classification, mean particle size, motion, and total mass of hydrometeors	DC-8
High altitude monolithic microwave integrated circuit sounding radiometer (HAMSR)	B. Lambrigsten/Jet Propulsion Lab	Microwave radiometer	Microwave brightness temperatures in 25 channels, temperature, water vapor, liquid water profiles, and precipitation	DC-8
Meteorological measuring system (MMS)	P. Bui/NASA	Rosemont probes	In situ temperature, pressure, and wind field	DC-8
Langley Aerosol Research Group Experiment (LARGE)	B. Anderson and G. Chen/NASA	In situ aerosol sensors	Aerosol size distribution, number density, surface area, mass loading, extinction, and single scattering albedo	DC-8
LASE	E. Browell, S. Ismail, and R. Ferrare/NASA	Lidar	Water vapor mixing ratio, aerosol scattering, relative humidity, precipitable water, aerosol backscatter, and extinction	DC-8
Research Environment for Vehicle-Embedded Analysis on Linux (REVEAL)	L. Freudinger/NASA	Data acquisition, processing, and transmission	Real-time data feeds, and communications between airplane and ground operations	DC-8
GPS dropwindsondes	J. Halverson and G. Heymsfield/NASA, J. Dunion/NOAA	Aircraft-deployed sondes	Vertical pressure, temperature, humidity, and wind profiles	DC-8, NOAA G-IV, and NOAA P-3 Orion
Airborne expendable bathythermographs (AXBTs)	J. Dunion/NOAA	Aircraft-deployed bathythermographs	Sea surface temperature and subsurface ocean temperatures	NOAA P-3 Orion
Stepped frequency microwave radiometer (SFMR)	J. Dunion/NOAA	Passive microwave radiometer	Surface wind speed (over ocean) and rain rates	NOAA P-3 Orion
Lower fuselage radar	J. Dunion/NOAA	C-band radar	Radar reflectivity, radial velocity, and spectral width	NOAA P-3 Orion
Tail Doppler radar	J. Dunion/NOAA	X-band Doppler radar	Radar reflectivity and 3D winds, and spectral width	NOAA P-3 Orion

from Africa with their usual regularity. During the NASA DC-8 deployment on Sal, Cape Verde, seven well-defined waves were sampled by the DC-8 and surface-based assets. As anticipated, some waves developed and some did not: two became Debby and Helene, two never developed beyond the wave stage, and three had a more complex evolution, arguably having some connection with the development of Ernesto, Florence, and Gordon. The NAMMA database is being used to try to distinguish the reasons for the different fates of these seven AEWs. Here, we briefly summarize the structure of all seven waves as they passed Cape Verde's islands, and then we show AEW 1 in more detail, which failed to develop during the period of study. Snapshots of the two developing systems sampled during NAMMA are shown: Debby as a tropical storm (NASA and NOAA) and Helene as a tropical depression (TD; NASA), and later as a

hurricane (NOAA). Later sections give highlights of early results from the sampling of the Saharan air layer, and studies of the African dust and its effect on cloud microphysics.

Overview of the seven AEWs of NAMMA. Figure 2 illustrates the value of frequent special soundings from Praia, Cape Verde, taken 6 times daily. It also illustrates some ambiguities of any time series from a single location. Wave AEW 1 is apparent by the meridional (V) wind change at low levels ($\sim 850\text{--}1000$ hPa) but not at midlevels (above 800 hPa), while the opposite is true for wave AEW 6. However, the V wind change is neither necessarily indicative of the strength of the AEW nor of the vorticity center; wave AEW 2 (pre-Debby) and wave AEW 7 (pre-Helene) are not obviously stronger. Neither is the V wind change highly correlated with other aspects of

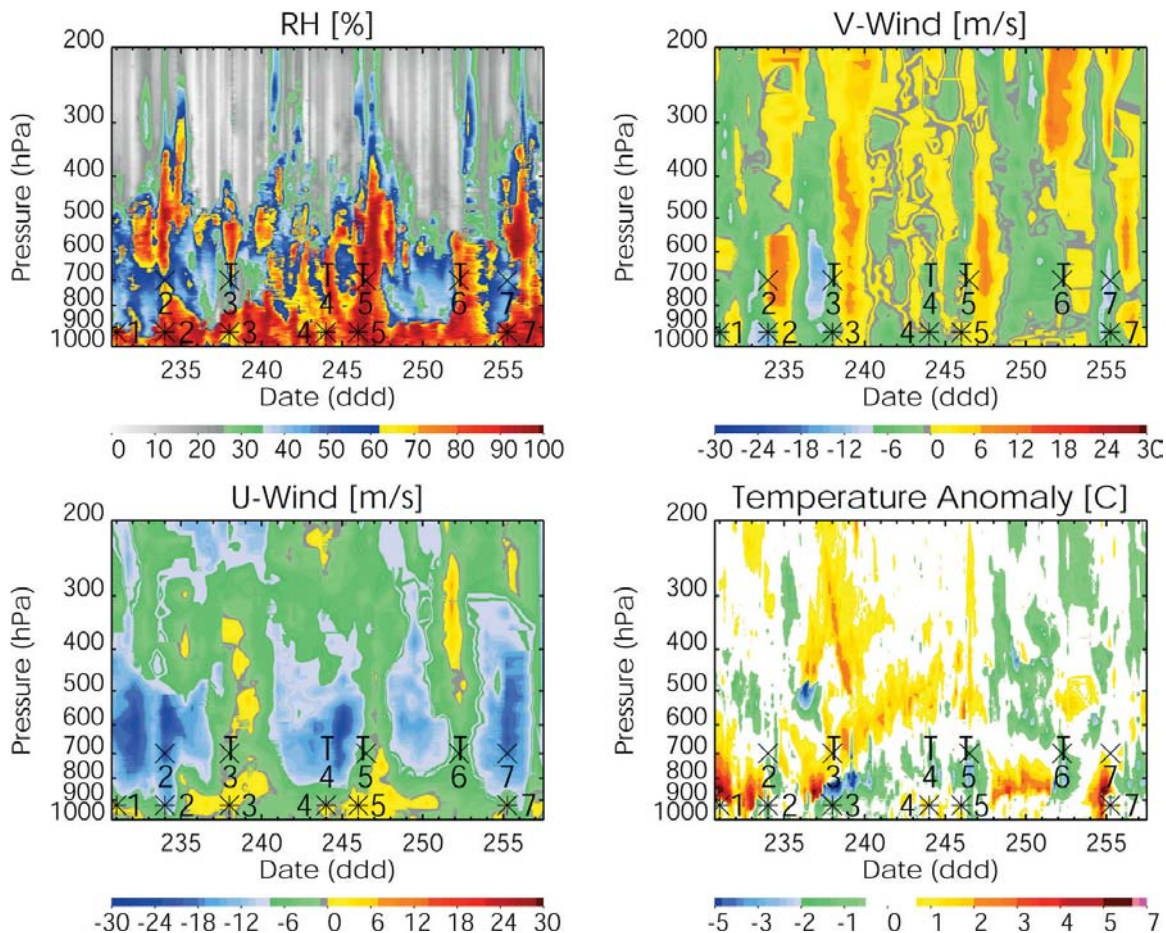


FIG. 2. Praia rawinsonde time series of (top left) RH, (top right) V wind, (bottom left) U wind, and (bottom right) temperature for the period between 1700 UTC 18 Aug (day 230) and 15 Sep 2006 (day 258). Here “X” indicates the passage time of an analyzed 700-hPa vorticity maximum, the “T” indicates the passage time of a 700-hPa wave trough, and the asterisk indicates the passage time of a 925-hPa vorticity maximum. Numbers indicate AEWs 1–7.

the height–time series, such as the enhancement of relative humidity or the zonal (U) wind changes. The temperature variations are included for completeness but are difficult to interpret. The aircraft missions are needed to add spatial detail.

Nondeveloping AEW 1. AEW 1 passed Cape Verde’s islands on 19 August 2006 and was flown by the DC-8 on both 19 and 20 August. Figure 3 illustrates a typical but important distinction between the AEW and the vorticity centers within the wave, as noted by Thorncroft and Hodges (2001) and Kerns et al. (2008): The AEW is larger scale and longer lived than its constituent vorticity maxima. Further, any development leading to tropical cyclogenesis must involve intensification of such a vorticity maximum (Montgomery et al. 2006; Dunkerton et al. 2008).

The main point to note is that the wave axis evolves from a north–south orientation to a northwest–southeast orientation over time, and starting on 19 August, the wave axis outruns the low-level (925 hPa) vorticity center along 16°N. By 21 August it outruns the midlevel (700 hPa) vorticity center along 10°N. The large latitudinal separation between the northern and southern vorticity maxima is typical of some (though not all) AEWs and may be one of the manifestations of the two AEW tracks (north versus south) often mentioned in the literature. Figure 4 shows the structure of AEW 1 at the time

of the second DC-8 flight after 1200 UTC 20 August 2006.

Figure 4 also demonstrates that according to the Global Data Assimilation System (GDAS; National

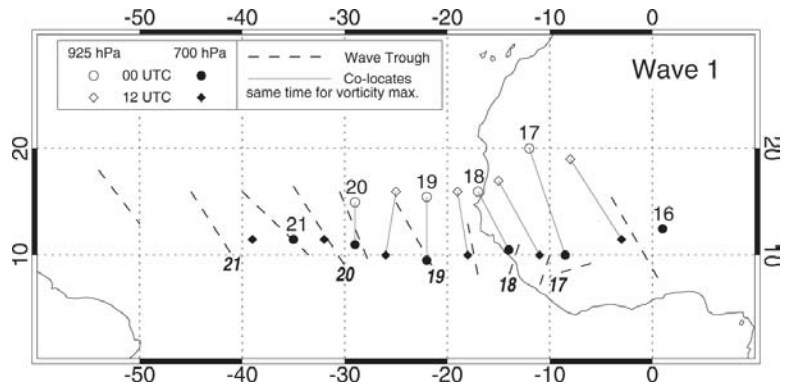


FIG. 3. Vorticity maxima tracks within AEW 1 at 925 hPa (open symbols) and 700 hPa (closed symbols) for 0000 (circle) and 1200 UTC (diamonds), as well as the 700-hPa wave trough axis (dashed line). Nonitalic numbers indicate the day of the month (at 0000 UTC) for the vorticity maxima, italic numbers indicate the day of the month for the 700-hPa wave trough (at 0000 UTC), and solid lines connect similar times.

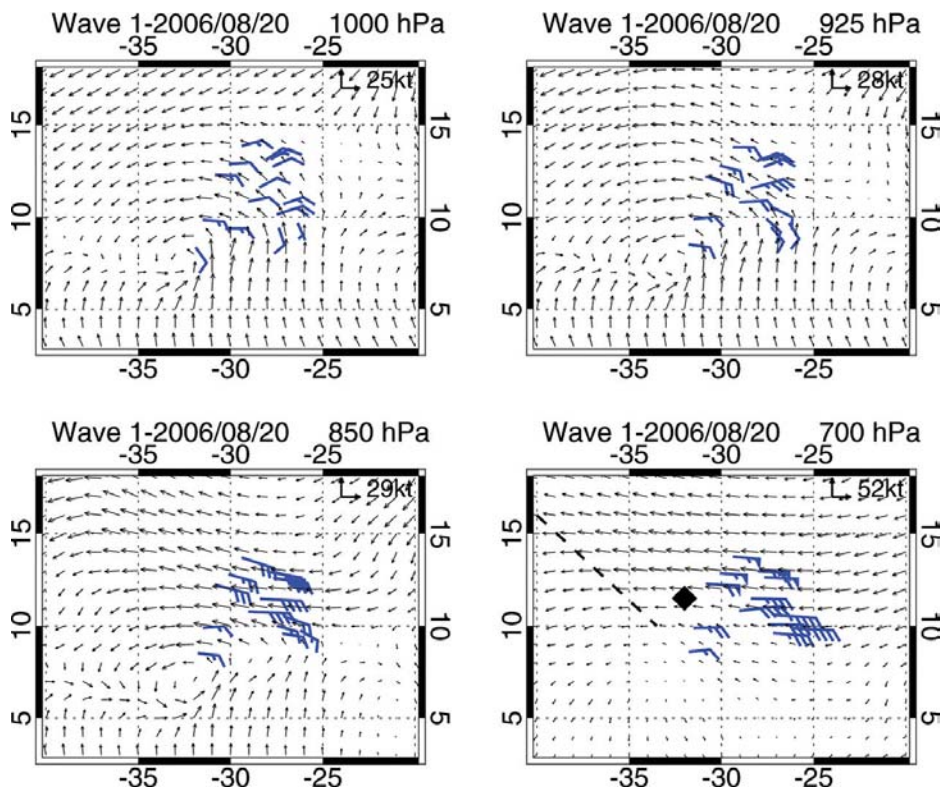


FIG. 4. GPS dropwindsonde winds (barbs) and GDAS analysis winds (vectors) for the second flight of AEW 1 on 20 Aug 2006. At this time, the original vorticity maximum tracking west near 10°N according to GDAS (Fig. 3) is still present and has apparently extended downward to 1000 hPa.

Center for Environmental Prediction) analysis, the northern part of AEW 1 as identified at 700 hPa had indeed outrun the main remaining vorticity

maximum, which is now well marked from 700 to 1000 hPa near 8°N, 32°W. There is no continuity between this vorticity maximum and the original 925-hPa feature that dissipated along 16°N (Fig. 3). The comparison with the GPS dropwindsonde winds also shows considerable disagreement between the observations and the model data north of 10°N, illustrating that one should not accept the GDAS analysis uncritically and that the details of both AEWs and vorticity centers have inaccuracies. Nonetheless, the satellite sequence (Fig. 5) can be used to illustrate some of the main features of AEW 1.

Figures 3 and 5 indicate the possibility that the weak system marked on the inter-tropical convergence zone (ITCZ) as AEW 1 may indeed be associated with the genesis of Tropical Storm (TS) Ernesto. From a location near 10°N, 48°W on 23 August the continued westward motion of AEW 1 is consistent with the Ernesto genesis location near 12°N, 63°W on 25 August 2006, although no convection was able to develop in the original wave north of the ITCZ, probably as a result of its being embedded in the dry SAL. At the same time, the rapid development of Debby almost immediately after AEW 2 (pre-Debby) exits the coast is obvious, as well as the close proximity of the SAL.

Figures 3 and 5 indicate the possibility that the weak system marked on the inter-tropical convergence zone (ITCZ) as AEW 1 may indeed be associated with the genesis of Tropical Storm (TS) Ernesto. From a location near 10°N, 48°W on 23 August the continued westward motion of AEW 1 is consistent with the Ernesto genesis location near 12°N, 63°W on 25 August 2006, although no convection was able to develop in the original wave north of the ITCZ, probably as a result of its being embedded in the dry SAL. At the same time, the rapid development of Debby almost immediately after AEW 2 (pre-Debby) exits the coast is obvious, as well as the close proximity of the SAL.

AEW 2: Tropical Storm Debby, its rapid development, unusual structure, and how the SAL may have helped to destroy it. As shown in Fig. 5, Debby formed quickly after its difficult-to-track parent AEW emerged from Africa as a significant vorticity center, probably not

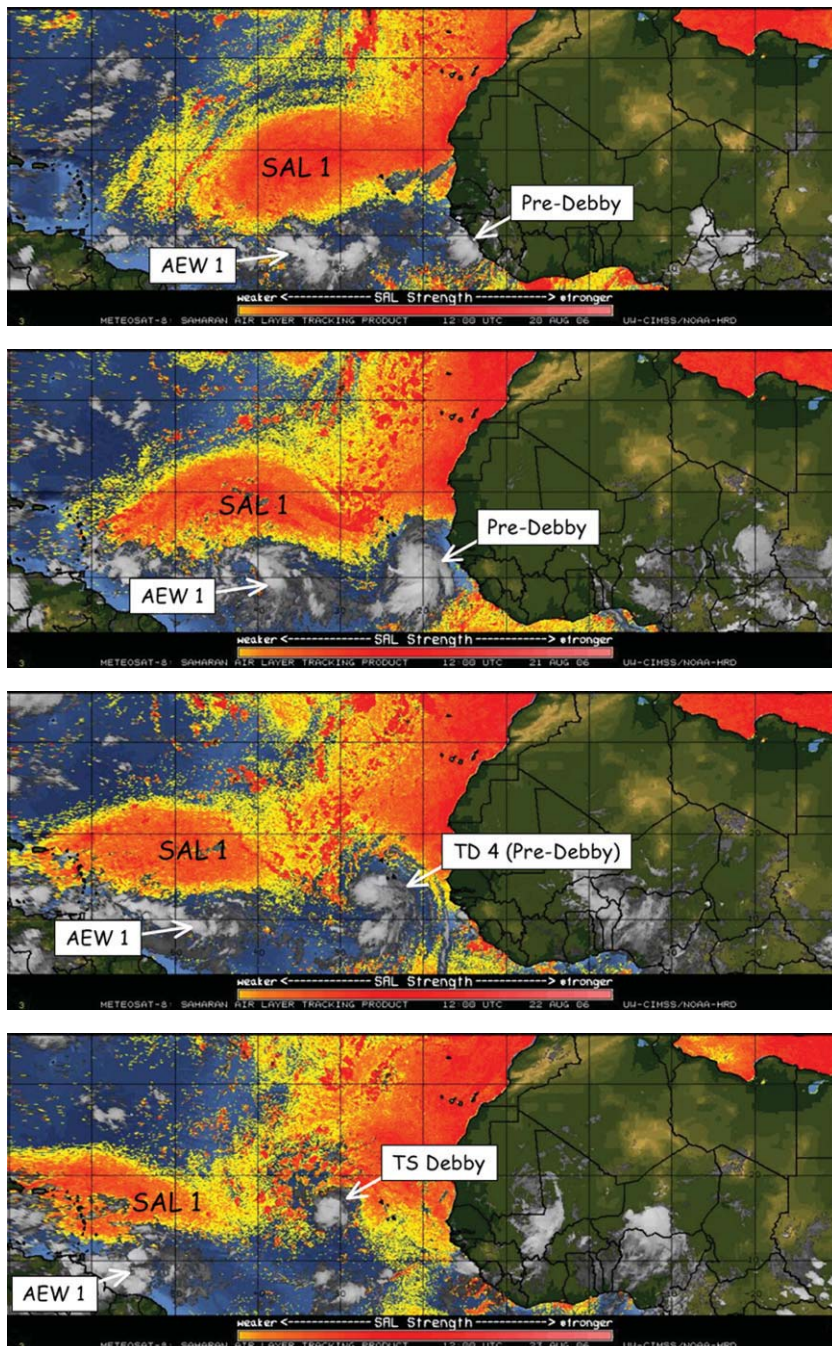


FIG. 5. Geostationary Operational Environmental Satellite (GOES) SAL-tracking satellite imagery at 1200 UTC from (top) 20 to (bottom) 23 Aug. The yellow-red shading indicates likely SAL regions with increasing amounts of dust content and dry lower-tropospheric air, as detected by the GOES imagery. On 20 Aug (flight data in Fig. 4) the weak AEW axis at 700 hPa (Fig. 3) is embedded in the SAL I near 38°W but deep convection associated with a new vorticity center at low levels (Fig. 3, AEW 1) is near 8°N. The small cloud system (pre-Debby) on the coast on 20 Aug quickly intensifies on 21 Aug, reaches TD strength on 22 Aug, and becomes TS Debby on 23 Aug.

coincidentally following a strong convective blow up near the coastline near 10°N. The DC-8 had just completed two consecutive missions (Table 2) in AEW 1, so unfortunately the first mission into AEW 2 (pre-Debby) could not take place until Debby had formed, about 24 h after being named a tropical cyclone. This mission on 23 August 2006 (Fig. 6) began with three passes across the storm at 237 hPa, with GPS dropwindsondes and remote sensing documenting the larger-scale storm structure, followed by three shorter passes near 695 hPa for obtaining detailed data in the storm core.

On the very first long leg passing through the storm from the north-northeast to the south-southwest (1320–1400 UTC), the second-generation Airborne Precipitation Radar (APR-2) data revealed a major surprise. The radar cross section (Fig. 7) showed an extraordinarily shallow structure resembling an eyewall, but tilted from the north-northeast to south-southwest with height, indicating strong environmental wind shear, also consistent with the GPS dropwindsonde wind measurements (not shown). This strong shear in the 5–8-km layer (blue ellipses) inhibited convection (maximum updrafts of only 5 m s⁻¹), covered the eye with cloud aloft, and determined the shallow structure of the storm. Available data collected between 1300 and 1600 UTC show a storm with a relatively small area in the southern side of the eye (red ellipse in Fig. 7) of active but weak convection and ice habits dominated by graupel; a widespread region of stratiform rain

with large aggregates aloft and a well-defined melting layer between 4500 and 3800 m MSL; and a dry sector northwest of the center with shallow, warm rain cells

TABLE 2. NAMMA flight summary.		
Date (2006)	Aircraft	Objective
15 Aug	DC-8	Ferry to Sal, Cape Verde
19 Aug	DC-8	Wave 1 (pre-Ernesto?), dust, A-Train underflight
20 Aug	DC-8	Wave 1 (pre-Ernesto?), dust, A-Train underflight
23 Aug	DC-8	Wave 2 (TS Debby), detailed structure, dust in environment
25 Aug	G-IV	TS Debby–SAL interaction
25 Aug	DC-8	Wave 3, nondeveloping dust, intercomparison with U.K. BAe146
26 Aug	G-IV	TS Debby–SAL interaction
26 Aug	DC-8	Wave 3, nondeveloping dust, A-Train underflight
30 Aug	DC-8	Cloud microphysics, dust
1 Sep	DC-8	Wave 4 (pre-Florence?)
3 Sep	DC-8	Wave 5 (pre-Gordon?)
4 Sep	DC-8	Wave 5 (pre-Gordon?)
5 Sep	DC-8	Dust flight over Atlantic and over Africa
8 Sep	DC-8	Wave 6 (nondeveloping)
9 Sep	DC-8	Wave 6 (nondeveloping)
12 Sep	DC-8	Wave 7 (TD, became Helene), dust entrainment
14 Sep	DC-8	Ferry to United States
15 Sep	G-IV	Hurricane Helene–SAL interaction
16 Sep	G-IV	Hurricane Helene–SAL interaction
18 Sep	P-3/G-IV	Hurricane Helene–SAL interaction
20 Sep	P-3/G-IV	Hurricane Helene–SAL interaction

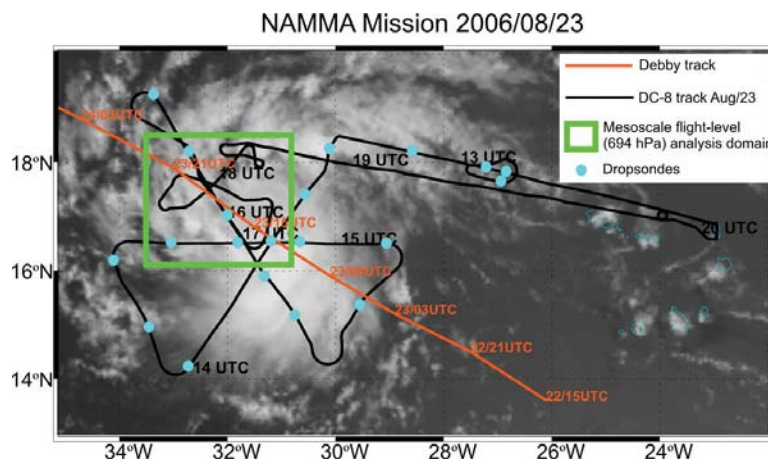


FIG. 6. DC-8 flight track on 23 Aug. The longer legs passing near the storm center (1320–1630 UTC) obtained remote-sensing and dropwindsonde data from 237 hPa before descending to near 700 hPa to obtain detailed in situ data across the storm core. The best track for Debby from 22 to 24 Aug is in red.

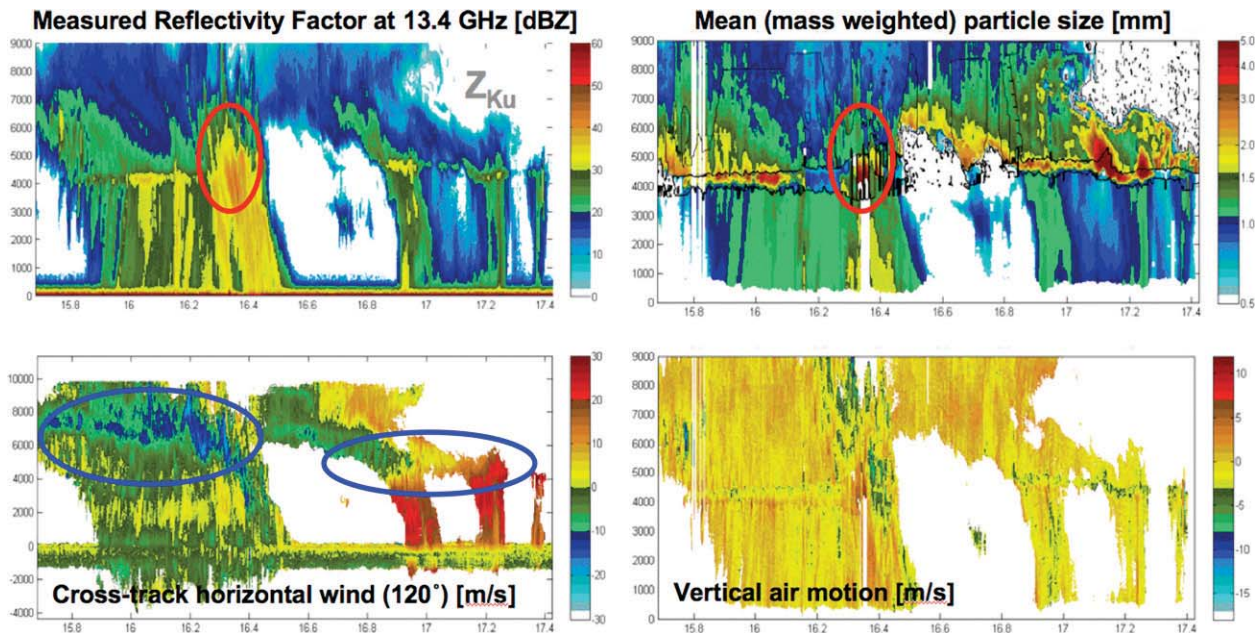


FIG. 7. (right) North-northeast to (left) south-southwest along-track sections from APR-2 across the center of Debby, acquired between 1328 and 1345 UTC on 23 Aug. All plots have coordinates of latitude (x axis, °) and altitude (y axis, m) and are collocated in space and time. (upper left) Equivalent reflectivity factor at 13.4 GHz. (lower left) Cross-track horizontal wind, a derived quantity from the Doppler measurements. (upper right) Mean particle size and (lower right) vertical air motion are retrieved quantities generated by a Bayesian scheme applied to the full set of APR-2 measurements. The red ovals highlight the region of modest convective activity with likely presence of graupel below 6-km MSL, and the blue ovals highlight the midlevel regions of high wind shear.

(not shown). Lidar Atmospheric Sensing Experiment (LASE) aerosol data (Fig. 8) indicate that African dust may have been impinging on the storm in this dry sector and also in the southwest quadrant. Retrievals of mean particle size from dual-frequency polarimetric measurements highlight the presence of large aggregates in the northeast sector, likely resulting from advection of uplifted hydrometeors in the convective area. There are corresponding in situ microphysics observations at flight altitude.

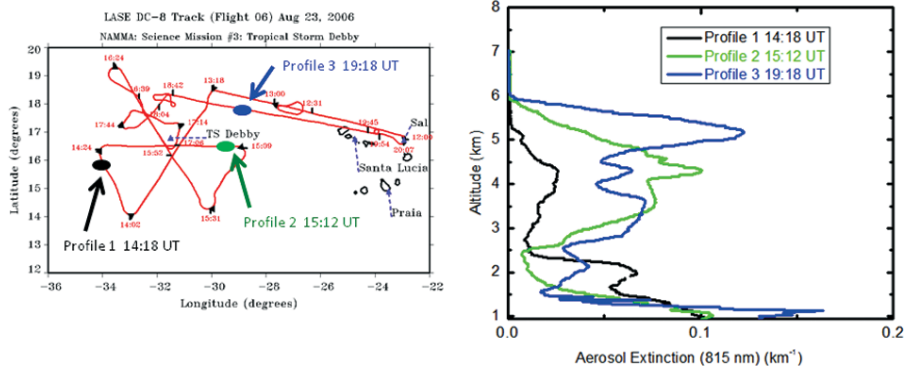


FIG. 8. Flight track for the Debby mission showing (left) locations of LASE profiles of aerosol extinction and (right) profiles. Compare with satellite image of Debby (Fig. 6).

A major question is whether Debby was near its maximum intensity at this time, or whether it was already weakening. There is a clear need for high-resolution modeling studies to address these questions and to help elucidate whether such a shallow tropical cyclone, with strong vertical wind shear near its center, has the potential for additional strengthening and if so, under what circumstances. Despite the shallow eyewall and highly sheared structure, the penetration data from near 700 hPa (Fig. 9)

reveal a warm core with a 4°–6°C temperature rise in the center, a visible eye surrounded by convective clouds, and a wind maximum on the east side exceeding 30 m s⁻¹.

The NOAA/Atlantic Oceanographic and Meteorological Laboratory (AOML)/Hurricane Research Division conducted its first Saharan Air Layer Experiment (SALEX) mission around Tropical Storm Debby on 25 August

2006 with the NOAA G-IV high-altitude jet (less than 2 days after NASA conducted its TS Debby DC-8 mission). The main objectives of SALEX include improving the understanding and prediction of how the SAL's dry air, midlevel easterly jet, and suspended mineral dust affect Atlantic TC intensity change, and assessing how well these components of the SAL are being represented in forecast models. The data collected during the Debby and Helene NOAA SALEX missions were designed to complement the observations collected "upstream" in these storms by NASA assets. The cooperative nature of these NOAA and NASA research activities provided an unprecedented east-west sampling of AEWs/TCs and SAL outbreaks and the interactions that frequently occur between these phenomena. Detailed mission summaries, GPS dropwindsonde data, and satellite imagery related to the NOAA G-IV TS Debby SALEX missions can be found online (www.aoml.noaa.gov/hrd/Storm_pages/debby2006/).

Figure 10 shows a mosaic of total precipitable water (TPW) derived from microwave satellite imagery along with the 25 August G-IV SALEX flight track and GPS dropwindsonde points. The satellite imagery indicates that TS Debby was completely surrounded by a large SAL outbreak (SAL 2), which is also evident from several GPS dropwindsondes launched by the G-IV during the SALEX mission (Fig. 10). These GPS dropwindsonde profiles indicate that midlevel (~500–850 hPa) relative humidity (RH) in these SAL regions was as low as 10%–15%. Additionally, profiles of RH from collocated Global Forecast System (GFS) and Geophysical Fluid Dynamics Laboratory (GFDL) model analyses suggest that although both models were capturing the general moisture trends below, within, and above the SAL, they tended to underestimate the SAL's midlevel dryness. For the small sample shown, GFS and GFDL overestimated the SAL's midlevel moisture by as much as 40%–50% RH.

AEW 7: 12 September 2006 flight into tropical depression (TD 8: pre-Helene). This was the first and only DC-8 flight into AEW 7 that later developed into Hurricane Helene. During the flight, the National Hurricane Center (NHC) classified this storm as TD 8 and forecasted that the storm would reach category 1 intensity in 2 days. This AEW had been followed over the continent for several days, and there were earlier reports of strong mesoscale convective systems passing by the MIT radar located much farther inland near Niamey, Niger. The flight planning on the previous day was designed to study this AEW as it reached the coast, because there was evidence from

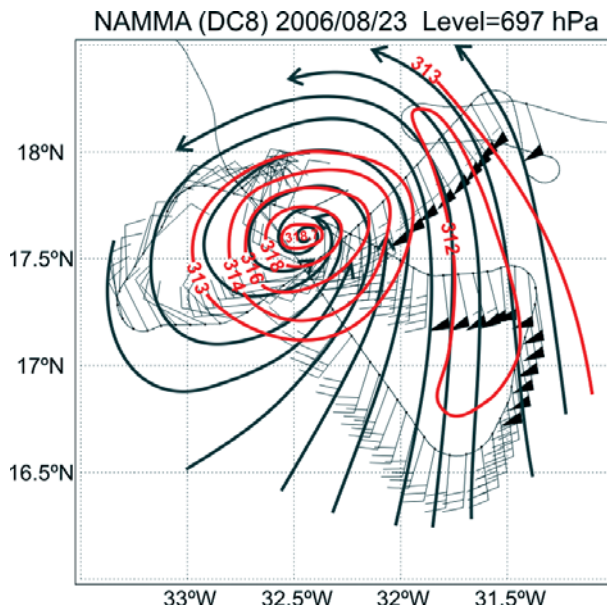


Fig. 9. Inner core structure of TS Debby from ~700-hPa DC-8 flight-level data near 700 hPa centered near 1700 UTC 23 Aug. Red lines indicate potential temperature, thick gray lines are streamlines, thin gray line is the aircraft track, and each full wind barb is 10 kt, each flag 50 kt.

the visible satellite data of a weak vortex over land. By the morning of the flight, the apparent wave axis and circulation had already cleared the coast with roughly 12° westward movement in just 1 day. Dry air intrusion was beginning on the north side near Sal. NAMMA mission scientists decided to fly a more generic flight pattern on 12 September with two main passes across the estimated circulation center, sampling the larger-scale flow, sampling the SAL on the north side, and developing a module to map the vortex winds and thermodynamics near 700 hPa, as was done during the Debby mission (Fig. 11).

The contrast between the inner core structure of Debby (Fig. 9) and pre-Helene (Fig. 11) is striking. Although the larger-scale vortex size and strength were comparable, pre-Helene had weaker inner core winds and a cool center near 700 hPa instead of the anticipated TC warm core structure. The winds were even weaker near the surface, at less than 5 m s⁻¹. Because of a lightning strike to the aircraft near the end of this mission, this flight became the last DC-8 mission of NAMMA, and thus there is no direct evidence of the time scale which the warm core actually developed.

There were a number of interesting features of the overall storm and circulation observed with the DC-8 measurements, illustrated by the cover photograph and the 2D image of Fig. 12. During the first part

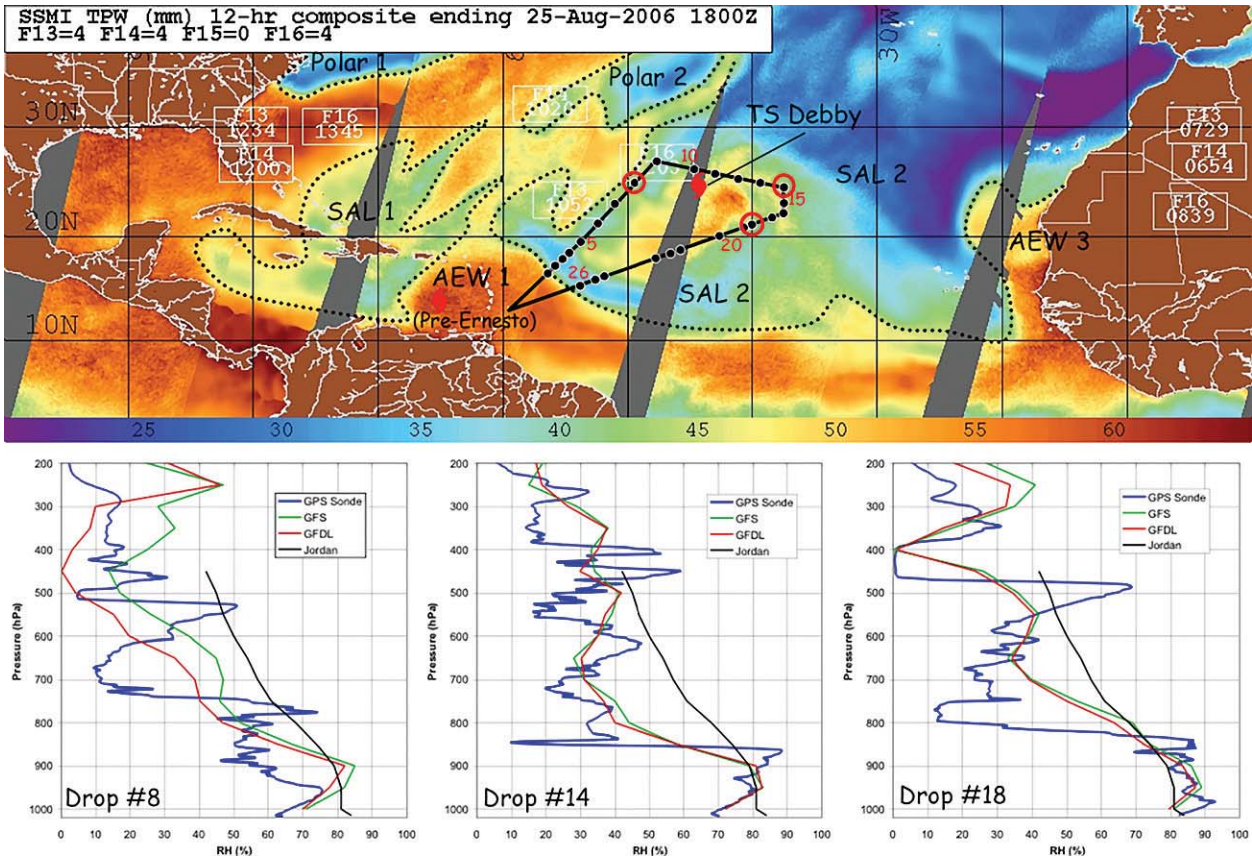
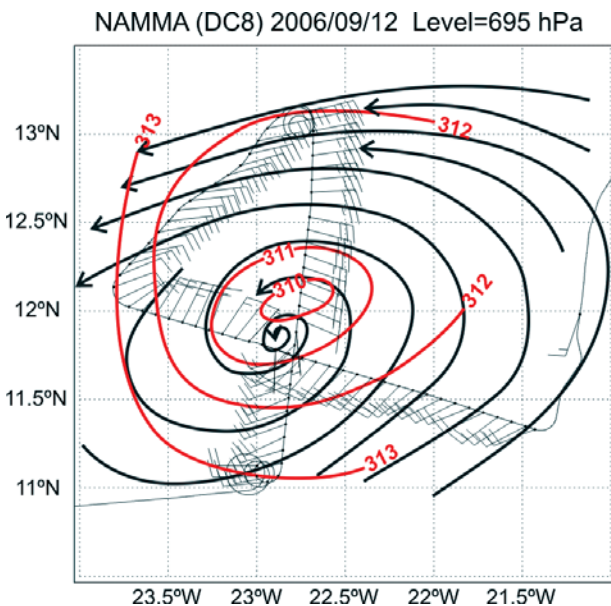


FIG. 10. (top) Mosaic of TPW from the constellation of Special Sensor Microwave Imager (SSM/I) satellites (1800 UTC 25 Aug). Regions where TPW values of <45 mm (dotted lines) indicate dry air in the low-to-mid-levels of the atmosphere (~600–925 hPa). Two distinct areas of dry SAL air (SAL I and SAL 2), two areas of dry polar air (Polar I and Polar 2), AEW I, and TD 5 are indicated in the imagery. The SALEX G-IV flight track and dropwindsonde points are overlaid on the imagery. Debby was located at ~24.4°N, 44.0°W at this time. (Imagery courtesy of NRL Monterey.) (bottom) GPS dropwindsonde profiles (blue curves) of RH (%) are indicated for drop numbers 8, 14, and 18. Collocated GFDL (red curves) and GFS (green curves) model analyses of RH and the Jordan mean moisture sounding (black curves) are also shown for each drop point.



of the flight near Sal, Cape Verde, the LASE instrument showed a deep dust layer up to 4-km altitude. Immediately east of this nearly cloud-free dust region, the DC-8 crossed over a strong convective line on the northwest side of the circulation center. This line propagated toward the northwest, was highly electrically active, and was also within distant range of the NASA TOGA radar. The juxtaposition of high, large dust aerosol concentrations immediately northwest of the storm, flowing into this intense convective line (Fig. 12), raises the question of whether the dust helped invigorate the convection, a hypothesis explored by Jenkins et al. (2008). Regardless of the effect on con-

FIG. 11. Inner core structure of AEW 7 as a tropical depression from DC-8 flight-level data near 700 hPa centered near 1600 UTC 12 Sep. See Fig. 9 for key to lines.

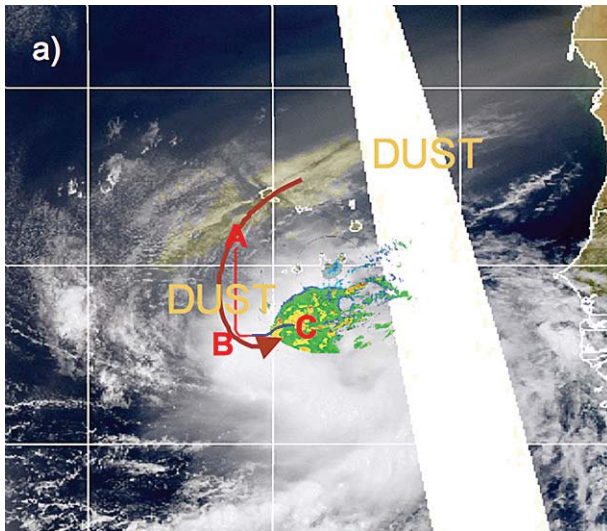
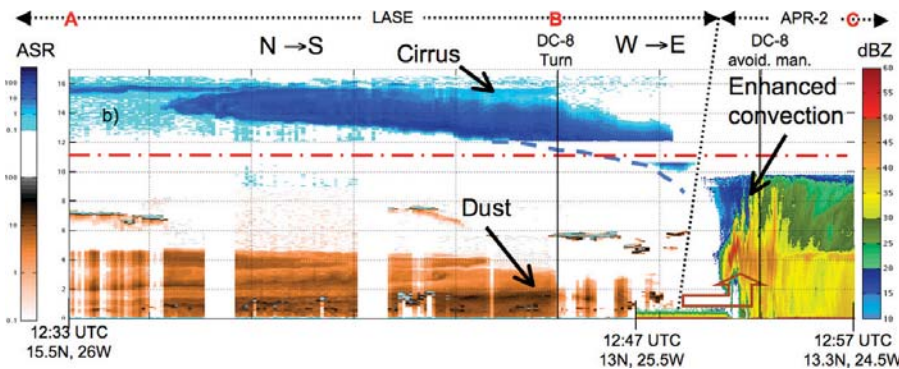


FIG. 12. Two-dimensional versions of the 3D cover image of TD8 on 12 Sep 2006, later to become Hurricane Helene. (a) Terra image shows the cloud system organized around the center of circulation just south of Cape Verde, together with the dust layer approaching from the Saharan region. The DC-8 approached the system from the northwest. The ground track is shown in red (LASE data available) and blue (APR-2 data available). Radar reflectivity from the TOGA radar on Praia is overlaid in the area within range and shows a line of convective cells along the western boundary of the storm. (b) (left) Vertical section of LASE's aerosol scattering ratio and (right) APR-2's Ku-band reflectivity. LASE data are attenuated when the DC-8 enters the cirrus shield (dotted line marks the approximate boundary). DC-8 path (red dashed-dotted line) and approximate cloud base (blue dashed line) are shown



for reference. (a),(b) The brown arrows indicate the likely path of the dust layer into the convective system. Dual-frequency radar observations show that small ice crystals dominated the cirrus "ahead" of the convective cells (blue area), while larger crystals and aggregates are present immediately "behind" it (green area).

vective vigor, the larger question of the effect of the dust (and the SAL) on TC development remains. Pre-Debby had a similar dust outbreak just to its northwest (Fig. 5). Although both systems eventually developed into TCs, their intensification may have been delayed by interactions with the SAL: Debby only peaked as a weak TS before dissipating and Helene took several days to reach hurricane strength.

NOAA conducted a series of G-IV and P-3 Orion SALEX missions in and around Helene, but these missions did not commence until 15 September, several hundred kilometers downstream from the Cape Verde region. Detailed mission summaries, GPS dropwindsonde data, aircraft radar composites, HRD H*Wind surface wind analyses, and satellite imagery related to the NOAA G-IV, and P-3 Orion TS/Hurricane Helene SALEX missions can be found online (www.aoml.noaa.gov/hrd/Storm_pages/helene2006/).

POSSIBLE ROLE OF BAROTROPIC ENERGY CONVERSION IN DISTINGUISHING DEVELOPING WAVES FROM NONDEVELOPING WAVES. Ross and Krishnamurti (2007)

studied Atlantic tropical cyclogenesis in relation to AEWs exiting the west coast of Africa. They examined AEWs by applying postprocessing routines to NCEP final (FNL) analyses. The barotropic energy conversion is defined by

$$-u'v' \frac{\partial[u]}{\partial y} - v'^2 \frac{\partial[v]}{\partial y} - u'w' \frac{\partial[u]}{\partial p} - v'w' \frac{\partial[v]}{\partial p}, \quad (1)$$

where the prime terms are departures of the respective variable at a point from the zonal mean of that variable, and the bracket indicates the zonal mean of the variable. The zonal mean is calculated over the longitudinal range 10°E–45°W. The first term in this expression is typically the dominant term, and it relates the transport of the westerly eddy flux of momentum into regions of the easterly wind maxima that results in barotropic growth. These terms indicate that barotropic energy conversions at 700 hPa can be a robust indicator for wave development for NAMMA AEWs. The AEWs that developed into Tropical Storms Debby and Helene, within the NAMMA domain, had strong and unambiguously positive barotropic energy conversions, whereas all

NAMMA-06 AND HUMAN CAPACITY BUILDING FOR THE UNITED STATES AND SENEGAL

Undergraduate and graduate students from the United States (University of Alabama in Huntsville, Florida State University, Howard University, University of Illinois, University of North Dakota, University of Oklahoma, Texas A&M University, University of Utah, University of Virginia) and Senegal UCAD were involved in the NAMMA campaign. Students received hands-on experience assisting with a variety of research efforts that were being conducted in the field (Fig. SB2). For example, in Cape Verde, students were involved in aircraft and forecasting activities; in Senegal, students were involved in ground measurements (Fig. SB3). Faculty and research scientists at the Laboratory for Atmo-

spheric and Oceanic Physics—Simeon Forgang (LPAO—SF) also played an important role in obtaining data (radar, chemistry, forecasting) in Senegal and were responsible for upper-air measurements in Conakry, Guinea. In 2007, a workshop was held in Dakar, Senegal, to synthesize the data. From this meeting, synthesis teams were formed with two joint Senegalese/U.S. student posters on the squall line case of 11 September 2006.

An important component of the human capacity building is to increase the presence and participation of Senegalese and African-American students/scientists/faculty in the atmospheric sciences through field campaigns.

In geosciences, minorities were awarded less than 4% of doctorate degrees awarded between 1999 and 2004 (Williams et al. 2007). Building human and technical capacity in Africa remains a critical need for the atmospheric sciences (Jenkins et al. 2002; Washington et al. 2006), and the NAMMA/AMMA field campaign (Redelsperger et al. 2006) helped to address those needs with research going toward student theses, dissertations, and joint student–faculty publications (e.g., Jenkins et al. 2008; Jenkins and Pratt 2008; Grant et al. 2008).



FIG. SB1. (a) Graduate student Tamara Battle [Howard University (HU)] works with a NASA scientist on the DC-8. (b) Universite Cheikh Anta Diop (UCAD) graduate student Thioro Fall at the NPOL radar in Kawsara, Senegal.

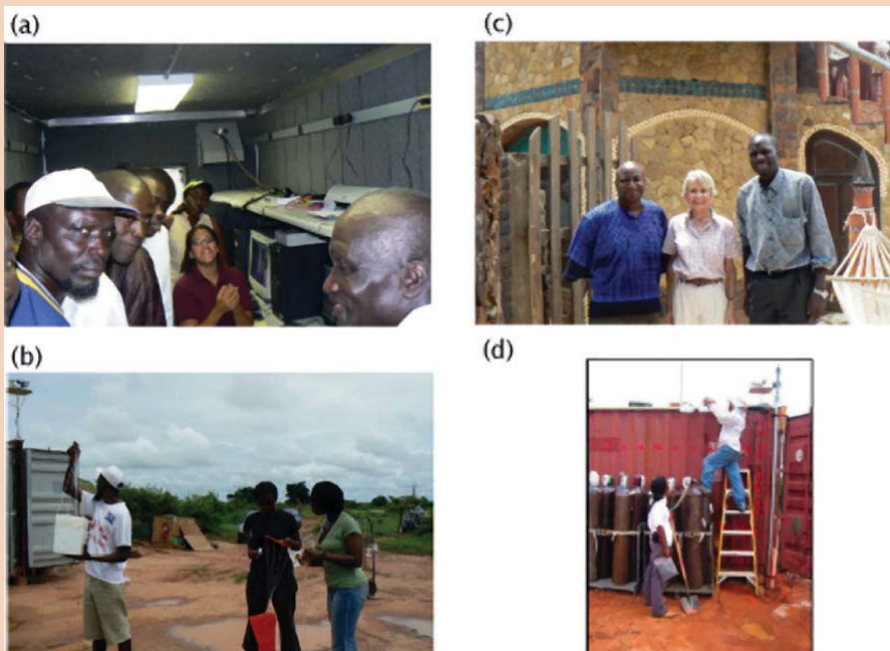


FIG. SB2. (a) Student Amber Reynolds explains radar images to Senegalese visitors. (b) Dr. Seydi Ndiaye and students Segayle Walford (HU) and Deanne Grant [University of Virginia (UVA)] launch an ozonesonde at Kawsara. (c) U.S. Ambassador Jane Kacobs with Dr. Amadou Gaye (UCAD) and Gregory Jenkins (HU). (d) UVA professor Jose D. Fuentes works with Deanne Grant at the research trailer in Kawsara, Senegal.

of the remaining waves had either neutral or negative barotropic energy conversions. The nondeveloping waves have a northwest–southeast tilt to the wave axis, a wind maximum behind the wave axis, and a

negative barotropic energy conversion. In contrast, the developing AEWs have a northeast–southwest tilt to the wave axis, a wind maximum ahead of the wave axis, and a strong positive barotropic energy

conversion. Additional studies are underway to test the hypothesis that barotropic growth is a significant factor in wave development.

THE SAL AND ITS ROLE IN AFFECTING CLOUD MICROPHYSICS.

As shown in some of the earlier figures, Saharan air layers were ubiquitous across much of the tropical Atlantic Ocean during the NAMMA period. The SAL is often adjacent to regions with deep convective clouds, sometimes clearly reaching them as in pre-Helene, sometimes not. Important objectives included documenting the characteristics of these aerosol layers and examining the influence of mineral dust on the formation and development of tropical clouds. To facilitate these studies, an extensive suite of in situ sensors aboard the DC-8 were used to measure particle size distributions, fractional volatility, number densities, and wavelength-/size-dependent optical properties. In addition to gathering a large set of background aerosol observations in this relatively unexplored region of the world, we sampled dust within the SALs on at least 11 occasions during six separate research flights. These visually evident, horizontally extensive layers typically resided between 2- and 4-km altitude over the ocean. They were characterized by having carbon monoxide mixing ratios of 75–80 ppbv, relatively low particle number concentrations (300–600 cm^{-3}), but scattering coefficients that at times exceeded 300 Mm^{-1} . Extinctions integrated over the depths of the layers yielded aerosol optical thicknesses ranging from 0.03 to 0.45, with a median of 0.13.

REMOTE AND IN SITU SAMPLING OF THE SAL: EXAMPLE OF 30 AUGUST 2006.

Aerosol data measured during a vertical descent through the SAL layer and into the marine boundary layer on 30 August are shown in Fig. 13. The vertical profile of particle number concentration and associated size distribution show that at least

two different aerosol size modes were present in the SAL: a small mode with a number mean diameter of 0.1–0.2 μm , and a larger mode with a number mean diameter of 0.7–0.8 μm . Although the small mode accounted for little of the particle mass, it contributed about 90% of the number concentration. The majority of the particles present in the SAL were nonvolatile at temperatures lower than 300°C, suggesting that even the small-mode particles were dominated by mineral dust. Twohy et al. (2009) showed that dust in the SAL may be slightly hygroscopic and act as cloud condensation nuclei (CCN) under some conditions. Thus, as discussed below, these high concentrations of submicron dust particles may influence microphysical properties of cloud systems interacting with the SAL.

With a volume mean diameter of 2–3 μm , the large dust mode was responsible for >75% of the optical extinction and nearly all of the mass loading. The prevalence of large, nonabsorbing dust particles in the layers resulted in scattering coefficients that were relatively constant with wavelength (e.g., near-zero Angstrom exponents) and single-scattering albedos that ranged from 0.96 to 0.97. These values are higher than those derived from AERONET data inversions (Dubovik et al. 2002), but consistent with other in situ Sahara dust observations recorded during the Saharan Mineral Dust Experiment (Schladitz et al. 2009) and suggest that the dust would have

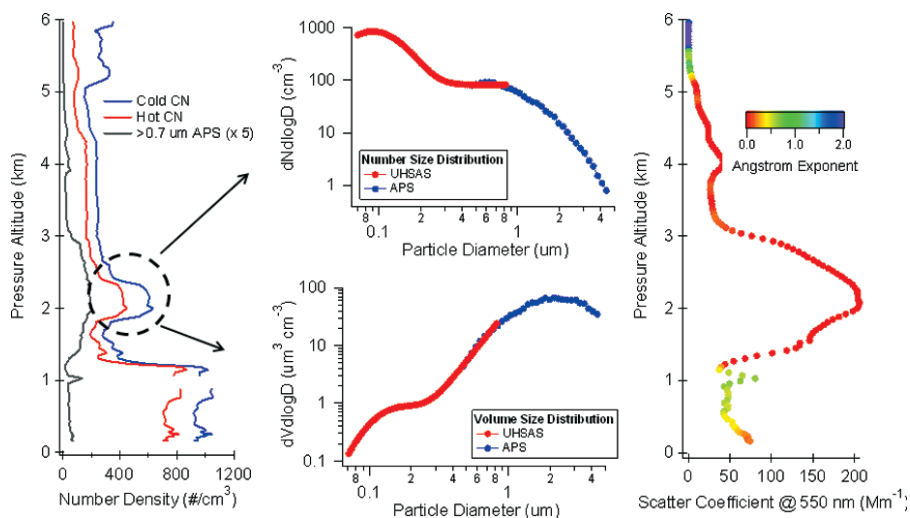


FIG. 13. Optical and physical properties of Saharan dust sampled during NAMMA flight 5 (30 Aug 2006). (left) Vertical concentration profile of CN particles of different types from 30 Aug 2006. Blue lines are particles larger than 0.01 μm (“cold CN”). Red lines are particles that were nonvolatile at temperatures below 300°C (“hot CN”). Black lines are particles that were larger than 0.7 μm (from the aerodynamic particle sizer, concentrations multiplied by 5). (top center) Dust number size distribution, and (bottom center) dust volume size distribution. (right) Vertical distribution of scattering coefficient and Angstrom exponent.

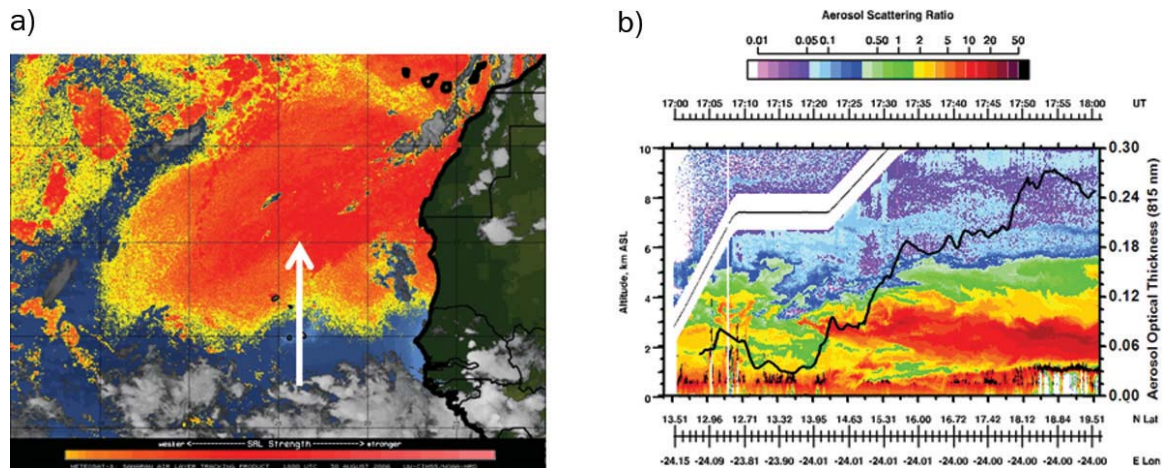


FIG. 14. (a) Meteosat image showing SAL layer strength at 1800 UTC 30 Aug 2006. White arrow denotes segment of DC-8 flight track as the aircraft flew from south to north into the SAL. (b) LASE aerosol optical thickness (815 nm) derived from LASE extinction profiles for the altitude region between 1.3 and 15 km is also shown by the black line (right axis). Note the presence of clouds at about 1 km in the SAL, signified by the intense returns that obscure most of the signal below.

only minor local heating effects. The differences in single-scattering albedo as well as in the wavelength dependence of absorption and scattering (Fig. 13) made it fairly easy to distinguish the dust particles from sea salt and pollution-related aerosols transported from distant sources.

On 30 August, the DC-8 flew from a less dusty region at 13°N (with an aerosol optical thickness of

about 0.03, integrated from 1.3 km to the lidar altitude) to a region at about 20°N that contained a much higher dust loading with an aerosol optical thickness of about 0.25 (Fig. 14). This case also presented an opportunity to sample in situ small cumulus clouds in the marine boundary layer at 20°N, with cloud tops about 1.3 km, beneath the main dust layer (Fig. 14). The number concentration of all particles in the

size range from 0.5- to 45- μm ambient diameter at 1.0 km is shown in black in Fig. 15a. In this size range, large sea salt and dust particles, as well as cloud droplets, are detected. The concentration of particles larger than about 3- μm diameter (predominately cloud droplets) is shown where the cloud passages are apparent.

The clear-air large aerosol concentrations of $\sim 25\text{--}200\text{ cm}^{-3}$, as well as the in-cloud droplet concentrations of $600\text{--}800\text{ cm}^{-3}$, are quite high for marine air. The latter are only slightly lower than the maximum available conden-

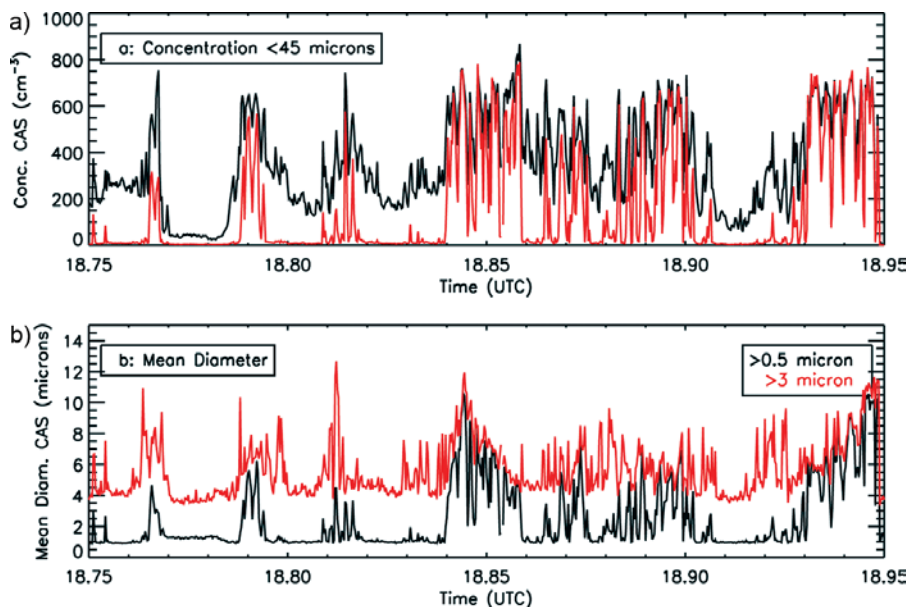


FIG. 15. (a) Number concentration of particles between 0.5 and 45- μm diameter (black line) and between 3.0 and 45- μm diameter (red line) for a flight leg through small cumulus clouds at 20.1°N on 30 Aug 2006. (b) Mean diameter for the 0.5–45- μm size range. Data are from the cloud aerosol and precipitation spectrometer (CAPS), a wing-mounted probe that measures particle sizes at ambient humidity.

SURFACE-BASED REMOTE SENSING AND IN SITU MEASUREMENTS AT CAPE VERDE: SMART-COMMIT

Although space-borne remote sensing observations (e.g., spectral imaging) cover large spatial domains, they are often plagued by contamination from surface signatures (e.g., variable reflectance). Thus, ground-based in situ and remote sensing measurements, where signals come directly from atmospheric constituents, the sun, and/or the Earth-atmosphere interactions, provide additional information content for comparisons that confirm quantitatively the usefulness of the integrated surface, aircraft, and satellite datasets. Two ground-based mobile laboratories, Surface-sensing Measurements for Atmospheric Radiative Transfer (SMART) and Chemical, Optical, and Microphysical Measurements of In-situ Troposphere (COMMIT), were deployed to Sal, Cape Verde, 2–26 September 2006 to measure atmospheric aerosols and constituent chemicals. To quantify the energetics of the surface-atmosphere system and the atmospheric processes, more than 50 instruments in SMART-COMMIT

(cf. <http://smart-commit.gsfc.nasa.gov>) fall into three categories: flux radiometer, radiance sensor, and in situ probe. As shown in Fig. SB3, several dusty events occurring nearly in weekly cycle were captured by the micropulse lidar (as well as by sky imager, sun photometer, and interferometer). When Saharan dust layers descend through the marine environment and reach the surface (e.g., episodes on 12 and 20 September 2006), in situ measurements of particle size distribution, mass concentration, and scattering/absorption coefficients at different relative humidity reveal distinct characteristics. Combining with back-trajectory analysis and satellite retrievals, Jeong et al. (2008) found that the deduced optical properties from in situ measurements differ significantly for dust particles originating from different source regions over North Africa. This emphasizes the importance of resolving dust properties in subregional scales to attain a better assessment of direct radiative effect by Saharan dust.

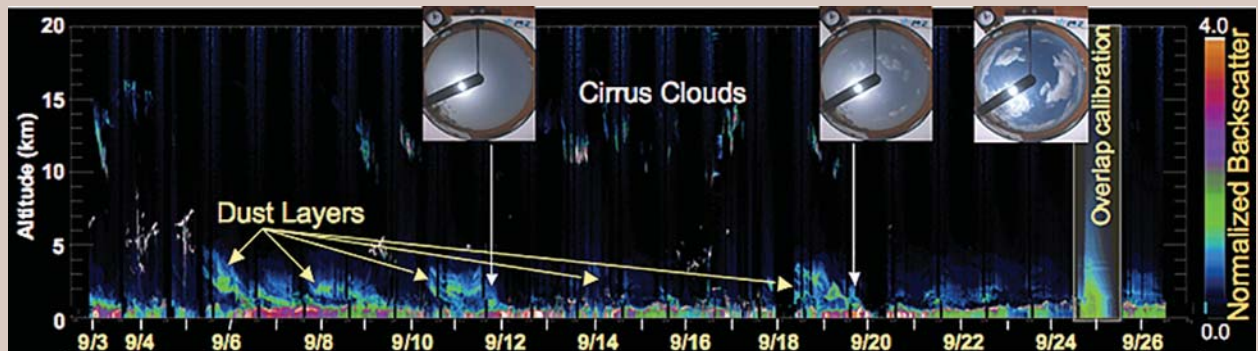


FIG. SB3. Time series of normalized backscatter intensity profiles measured by a micropulse lidar in SMART-COMMIT, based at Sal, Cape Verde, during 2 through 26 Sep 2006. Saharan dust layers aloft are depicted in green-to-light-blue colors around 1–4-km altitude, as well as frequently observed cirrus clouds (10–15 km) associated with large-scale atmospheric circulations. The total sky imager gives examples of sky conditions on 11 and 19 Sep for dusty days and on 25 Sep for relatively a dust-free day (all images at 1504 UTC).

sation nuclei (CN) concentrations shown in Fig. 13. Additionally, despite moderate liquid water contents of $0.2\text{--}0.8\text{ g m}^{-3}$, the mean droplet diameters (Fig. 15b) are small for maritime clouds, which could affect coalescence and precipitation development.

To evaluate what types of particles were acting as CCN in this case, cloud residual particles were collected with a counterflow virtual impactor (CVI; Noone et al. 1988; Twohy et al. 1997). The CVI collects and evaporates droplets larger than about $7\text{-}\mu\text{m}$ diameter while removing smaller, interstitial aerosol particles. Once collected by the CVI, droplets are evaporated and their nonvolatile residual particles are captured by a two-stage impactor. The small particle stage collected residual particles approximately

$0.1\text{--}0.5\text{ }\mu\text{m}$ in diameter, while the larger particle stage collected particles from about $0.5\text{ }\mu\text{m}$ up to several microns in size. After collection, particles were analyzed by electron microscopy and X-ray analysis to determine their chemical type, as in Twohy and Poellot (2005).

Residual particle composition from the clouds shown in Fig. 15 is displayed in Fig. 16. Slightly more than half of the droplets contained salts, probably reflecting sea salt generated with the relatively high wind speeds of $10\text{--}20\text{ m s}^{-1}$ present during this run. Eight percent of the residual nuclei was ammonium sulfate or bisulfate, while 3% was aluminosilicate dust particles with small amounts of potassium, calcium, and other components that occur naturally

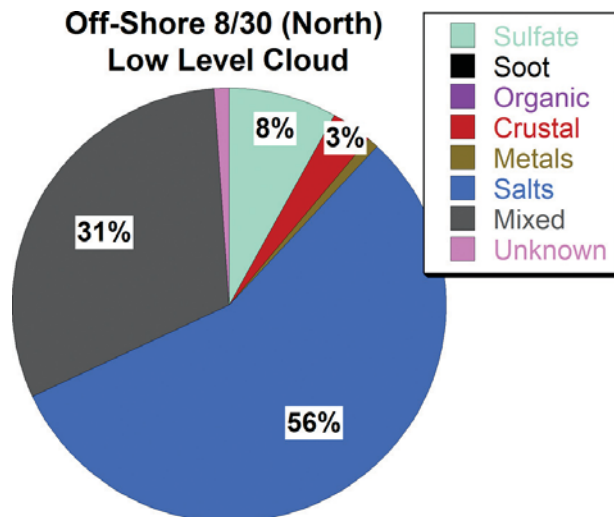


FIG. 16. Percentage by number of different particle types from cumulus cloud residual nuclei at 1 km, below the main dust layer at 20°N on 30 Aug 2006. Here, 100 particles, 50 from each of two size stages, were analyzed. For simplicity of display, percentages from both particle size categories (larger than ~0.1 and larger than ~0.5 μm) have been averaged. However, the larger particles contained higher fractions of mixed particle types, and most of the sulfate particles were in the smaller size range.

in some soils. Thirty-one percent of the residual nuclei was dust particles mixed with additional soluble material such as sodium or calcium salts and sulfate. Other small cumulus clouds sampled during the project also had approximately one-third of the droplets containing either pure dust or dust mixed with sulfates or sea salt. The mixed crustal dust particles are expected to act as cloud condensation nuclei because of their relatively large size and the presence of soluble material, which makes them more hygroscopic. Additionally, because many of the sampled crustal particles sampled contained not only silicon and aluminum but also potassium, calcium, and other naturally occurring cations, they are likely to be slightly hygroscopic even without the addition of soluble material from the atmosphere. It is well known that Saharan dust can act effectively as an ice nucleus (e.g., Field et al. 2006), but these particles apparently can act as cloud condensation nuclei as well (Twohy et al. 2009). The input of Saharan dust in the lower and midregions of deep convective clouds in the eastern North Atlantic is likely to affect ice microphysics, latent heat release, and possibly storm duration and lifetime (e.g., Khain et al. 2005).

For example, increased dust CCN may form smaller droplets, which freeze at higher altitudes,

invigorating the storm through latent heat release at higher levels. This could be the mechanism for enhanced convection as observed pre-Helene (Fig. 12). Although initially increasing convective intensity and precipitation amount, the low humidity and high shear influence of the SAL may ultimately inhibit precipitation and secondary development driven by convective downdrafts (e.g., Khain et al. 2008). These influences will be examined through modeling studies using NAMMA measurements for input and validation.

PROMISING AREAS FOR FOLLOW-UP AND FUTURE RESEARCH.

The seven AEWs sampled during the NAMMA field campaign probably represent the best validation database ever obtained in the eastern North Atlantic. Therefore, it is an opportunity to evaluate the latest remote sensing retrieval algorithms, and dynamics and microphysics parameterizations used in numerical models, and to use the most advanced model simulations to attempt to answer the major question of tropical cyclogenesis: what is the relative importance of a favorable large-scale environment versus timely and well-placed development of intense convection near the incipient storm core? Although the final answer is probably more complicated than a simple “either/or,” this database promises new insights into how weak disturbances intensify (or do not) and the role played by the structure and evolution of the SAL, in this, the main development area for tropical cyclones in the Atlantic basin.

ACKNOWLEDGMENTS. The opportunity to create and graft a downstream extension to the AMMA program was made a reality by the vision and energy of Dr. Ramesh Kakar with the support of Dr. Jack Kaye, both of NASA headquarters. The NAMMA science team thanks Dr. Kakar for his support of the field program and the analysis phase. Participation of SMART-COMMIT was supported by Dr. Hal Maring, NASA Radiation Science Program. The NASA Micro-Pulse Lidar Network, led by Dr. E. J. Welton, was funded by the NASA Earth Observing System and Radiation Science Program. The contribution by Dr. Simone Tanelli was performed at the Jet Propulsion Laboratory, California Institute of Technology, under contract with NASA. Kudos to Michael Gaunce, Michael Craig, Marilyn Vasques, Sue Tolley, and the entire logistical support team from NASA Ames Research Center. The cooperation and support of the Cape Verde government, and their weather service, was invaluable, and special thanks are due to Dr. Jose Pimentalima. On the African continent, similar thanks are due to Jean-Blaise Ngamini,

Amadou Gaye, and so many others. Everette Joseph (Howard University) and Jose Fuentes (University of Virginia) were instrumental in carrying out the observational and student programs in Senegal. Student funding for activities reported in “NAMMA-06 human capacity building for the United States and Senegal” came from NASA Grant NNX06AC78G and NSF Grant OISE-0553959. The 6-times daily sounding program at Praia was led and carried out under the direction of Frank Schmidlin. The TOGA radar at Praia and the NPOL radar at Kawsara were installed and operated under the leadership of John Gerlach. The DC-8 crew and support team deserve special thanks for a remarkably successful operation. John Mejia and Jon Zawislak contributed several figures.

REFERENCES

- Burpee, R. W., 1974: Characteristics of the North African easterly waves during the summers of 1968 and 1969. *J. Atmos. Sci.*, **31**, 1556–1570.
- Carlson, T. N., 1969: Some remarks on African disturbances and their progress over the tropical Atlantic. *Mon. Wea. Rev.*, **97**, 716–726.
- , and J. M. Prospero, 1972: The large-scale movement of Saharan air outbreaks over the northern equatorial Atlantic. *J. Appl. Meteor.*, **11**, 283–297.
- Chen, T. S., 2006: Characteristics of African easterly waves depicted by ECMWF reanalysis for 1991–2000. *Mon. Wea. Rev.*, **134**, 3539–3566.
- Dubovik, O., B. Holben, T. F. Eck, A. Smirnov, Y. J. Kaufman, M. D. King, D. Tanré, and I. Slutsker, 2002: Variability of absorption and optical properties of key aerosol types observed in worldwide locations. *J. Atmos. Sci.*, **59**, 590–608.
- Dunion, J. P., and C. S. Velden, 2004: The impact of the Saharan air layer on Atlantic tropical cyclone activity. *Bull. Amer. Meteor. Soc.*, **85**, 353–365.
- Dunkerton, T. J., M. T. Montgomery, and Z. Wang, 2008: Tropical cyclogenesis in a tropical wave critical layer: Easterly waves. *Atmos. Chem. Phys. Discuss.*, **8**, 11 149–11 292.
- Evan, A. T., J. P. Dunion, J. A. Foley, A. K. Heidinger, and C. S. Velden, 2006: New evidence for a relationship between Atlantic tropical cyclone activity and African dust outbreaks. *J. Geophys. Res.*, **33**, L19813, doi:10.1029/2006GL026408.
- , and Coauthors, 2008: Ocean temperature forcing by aerosols across the Atlantic tropical cyclone development region. *Geochem. Geophys. Geosyst.*, **9**, Q05V04, doi:10.1029/2007GC001774.
- Field, P. R., O. Mohler, P. Connolly, M. Kramer, R. Cotton, A. J. Heymsfield, H. Saathoff, and M. Schnaiter, 2006: Some ice nucleation characteristics of Asian and Saharan desert dust. *Atmos. Chem. Phys.*, **6**, 2991–3006.
- Fink, A. H., D. G. Vincent, P. M. Reiner, and P. Speth, 2004: Mean state and wave disturbances during Phases I, II, and III of GATE based on ERA-40. *Mon. Wea. Rev.*, **132**, 1661–1683.
- Grant, D. D., J. D. Fuentes, M. S. DeLonge, S. Chan, E. Joseph, P. Kucera, S. A. Ndiaye, and A. T. Gaye, 2008: Ozone transport by mesoscale convective systems in western Senegal. *Atmos. Environ.*, **42**, 7104–7114.
- Haywood, J. M., and Coauthors, 2003: Radiative properties and direct radiative effect of Saharan dust measured by the C-130 aircraft during SHADE: 1. Solar spectrum. *J. Geophys. Res.*, **108**, 8577, doi:10.1029/2002JD002687.
- Highwood, E. J., J. M. Haywood, M. D. Silverstone, S. M. Newman, and J. P. Taylor, 2003: Radiative properties and direct effect of Saharan dust measured by the C-130 aircraft during Saharan Dust Experiment (SHADE): 2. Terrestrial spectrum. *J. Geophys. Res.*, **108**, 8578, doi:10.1029/2002JD002552.
- Houze, R. A., Jr., and A. K. Betts, 1981: Convection in GATE. *Rev. Geophys. Space Phys.*, **19**, 541–576.
- Hsu, N. C., S.-C. Tsay, M. D. King, and J. R. Herman, 2004: Aerosol properties over bright-reflecting source regions. *IEEE Trans. Geosci. Remote Sens.*, **42**, 557–569.
- Jenkins, G. S., A. Kamga, A. Garba, A. Diedhiou, V. Morris, and E. Joseph, 2002: Investigating the West African climate system using global/regional climate model. *Bull. Amer. Meteor. Soc.*, **83**, 583–595.
- , and A. Pratt, 2008: Saharan dust, lightning and tropical cyclones in the eastern tropical Atlantic during NAMMA-06. *Geophys. Res. Lett.*, **35**, L12804, doi:10.1029/2008GL033979.
- , —, and A. Heymsfield, 2008: Possible linkages between Saharan dust and tropical cyclone rain band invigoration in the eastern Atlantic during NAMMA-06. *Geophys. Res. Lett.*, **35**, L08815, doi:10.1029/2008GL034072.
- Jeong, M.-J., S.-C. Tsay, Q. Ji, N. C. Hsu, R. A. Hansell, and J. Lee, 2008: Ground-based measurements of airborne Saharan dust in marine environment during the NAMMA field experiment. *Geophys. Res. Lett.*, **35**, L20805, doi:10.1029/2008GL035587.
- Karyampudi, V. M., and T. N. Carlson, 1988: Analysis and numerical simulations of the Saharan air layer and its effect on easterly wave disturbances. *J. Atmos. Sci.*, **45**, 3102–3136.
- , and H. F. Pierce, 2002: Synoptic-scale influence of the Saharan air layer on tropical cyclogenesis over the eastern Atlantic. *Mon. Wea. Rev.*, **130**, 3100–3128.

- Kerns, B., K. Greene, and E. J. Zipser, 2008: Four years of tropical ERA-40 vorticity maxima tracks. Part I: Climatology and vertical vorticity structure. *Mon. Wea. Rev.*, **136**, 4301–4319.
- Khain, A., D. Rosenfeld, and A. Pokrovsky, 2005: Aerosol impact on the dynamics and microphysics of deep convective clouds. *Quart. J. Roy. Meteor. Soc.*, **131**, 2639–2663.
- , P. N. BenMoshe, and A. Pokrovsky, 2008: Factors determining the impact of aerosols on surface precipitation from clouds: An attempt at classification. *J. Atmos. Sci.*, **65**, 1721–1748.
- Kuettner, J. P., and D. E. Parker, 1976: Report on the GATE field phase. *Bull. Amer. Meteor. Soc.*, **57**, 11–27.
- Lau, W. K. M., and K.-M. Kim, 2007a: Cooling of the Atlantic by Saharan dust. *Geophys. Res. Lett.*, **34**, L23811, doi:10.1029/2007GL031538.
- , and —, 2007b: How nature foiled the 2006 hurricane forecasts. *Eos., Trans. Amer. Geophys. Union*, **88**, doi:10.1029/2007EO090002.
- , and —, 2007c: Reply to comment on “How nature foiled the 2006 hurricane forecasts.” *Eos, Trans. Amer. Geophys. Union*, **88**, doi:10.1029/2007EO260010.
- Montgomery, M. T., M. E. Nicholls, T. A. Cram, and A. B. Saunders, 2006: A vortical hot tower route to tropical cyclogenesis. *J. Atmos. Sci.*, **63**, 355–386.
- Noone, K. J., J. A. Ogren, J. Heintzenberg, R. J. Charlson, and D. S. Covert, 1988: Design and calibration of a counterflow virtual impactor for sampling of atmospheric fog and cloud droplets. *Aerosol Sci. Technol.*, **8**, 235–244.
- Redelsperger, J.-L., C. D. Thorncroft, A. Diedhiou, T. Lebel, D. J. Parker, and J. Polcher, 2006: African Monsoon Multidisciplinary Analysis: An international research project and field campaign. *Bull. Amer. Meteor. Soc.*, **87**, 1739–1746.
- Reed, R. J., D. C. Norquist, and E. E. Recker, 1977: The structure and properties of African wave disturbances as observed during Phase III of GATE. *Mon. Wea. Rev.*, **105**, 317–333.
- Riehl, H., 1954: *Tropical Meteorology*. McGraw-Hill, 392 pp.
- Rosenfeld, D., Y. Ridich, and R. Lahav, 2001: Desert dust suppressing precipitation: A possible desertification feedback loop. *Proc. Natl. Acad. Sci. USA*, **98**, 5975–5980.
- Ross, R. S., and T. N. Krishnamurti, 2007: Low-level African easterly wave activity and its relation to Atlantic tropical cyclogenesis in 2001. *Mon. Wea. Rev.*, **135**, 3950–3964.
- Schladitz, A., T. Müller, A. Massling, N. Kaaden, K. Kandler, M. Ebert, S. Weinbruch, C. Deutscher, and A. Weidensöhler, 2009: In situ measurements of optical properties at Tinfou (Morocco) during the Saharan Mineral Dust Experiment SAMUM 2006. *Tellus*, **61B**, 64–78.
- Tanré, D., and Coauthors, 2003: Measurement and modeling of the Saharan dust radiative impact: Overview of the Saharan Dust Experiment (SHADE). *J. Geophys. Res.*, **108**, 8574, doi:10.1029/2002JD003273.
- Thorncroft, C., and K. Hodges, 2001: African easterly wave activity and its relationship to Atlantic tropical cyclone activity. *J. Climate*, **14**, 1166–1179.
- Twohy, C. H., and M. R. Poellot, 2005: Chemical characteristics of ice residual nuclei in anvil cirrus clouds: Evidence for homogeneous and heterogeneous ice formation. *Atmos. Chem. Phys.*, **5**, 2289–2297.
- , A. J. Schanot, and W. A. Cooper, 1997: Measurement of condensed water content in liquid and ice clouds using an airborne counterflow virtual impactor. *J. Atmos. Oceanic Technol.*, **14**, 197–202.
- , and Coauthors, 2009: Saharan dust particles nucleate droplets in eastern Atlantic clouds. *Geophys. Res. Lett.*, **36**, L01807, doi:10.1029/2008GL035846.
- Washington, R., and Coauthors, 2006: African climate change: Taking the shorter route. *Bull. Amer. Meteor. Soc.*, **87**, 1355–1366.
- Williams, Q. L., V. Morris, T. Furman, 2007: A real-world plan to increase diversity in the geosciences. *Phys. Today*, **60**, 54–55.
- Wong, S., A. E. Dessler, N. M. Mahowald, P. R. Colarco, and A. de Silva, 2008: Long-term variability in Saharan dust transport and its link to North Atlantic sea surface temperature. *Geophys. Res. Lett.*, **35**, L07812, doi:10.1029/2007GL032297.
- Zhang, H., G. M. McFarquhar, S. M. Saleeby, and W. R. Cotton, 2007: Impacts of Saharan dust as CCN on the evolution of an idealized tropical cyclone. *Geophys. Res. Lett.*, **34**, L14812, doi:10.1029/2007GL030225.